*Article*

# In-Situ Piezoelectric Effect for Augmenting Performance of Self-Powered ZnO-Based Photodetector

**Thi My Huyen Nguyen and Chung Wung Bark** *

Department of Electrical Engineering, Gachon University, 1342 Seongnam-daero, Sujeong-gu, Seongnam-si 13120, Gyeonggi-do, Republic of Korea; myhuyen.dho.k12@gmail.com
* Correspondence: bark@gachon.ac.kr

**Abstract:** In this study, an in-situ piezoelectric effect is integrated into a photoactive region to develop a self-powered ultraviolet photodetector based on a p-n junction of ZnO@Polyvinylidene fluoride (PVDF) and poly [9,9-dioctylfluorene-co-N-[4-(3-methylpropyl)]-diphenylamine] (TFB). A ZnO@β-PVDF nanocomposite is fabricated using PVDF with the β-phase as the polymer matrix and ZnO nanoparticles as fillers. The strong piezoelectricity of β-PVDF can facilitate the separation and transport of photogenerated electrons in the depletion area and considerably reduce the dark current when the device is polarized with an external bias, resulting in an improvement in the on/off ratio and detectivity. Under 365-nm UV illumination, the as-fabricated device exhibits a high detectivity of $4.99 \times 10^{11}$ Jones, an excellent on/off ratio (up to $2.75 \times 10^4$), and a fast response speed of 46/53 ms (rise/fall times). The device functions stably over approximately 1000 continuous on/off cycles and exhibits extremely long-lasting photostability when exposed to UV light. The findings demonstrate a promising strategy for enhancing the performance of photodetectors for industrial applications.

**Keywords:** ZnO nanoparticles; β-phase PVDF; ZnO@PVDF nanocomposite; piezoelectric effect; self-powered photodetector

## 1. Introduction

Ultraviolet photodetectors (UV PDs), commonly referred to as UV sensors, are optoelectronic devices that convert photon energy into electrical energy. Over the past half-century, numerous applications of UV PDs based on semiconductors in the Internet of Things (IoT) have been reported. Scientists have successfully implemented UV PDs in various state-of-the-art fields, such as secret wireless communication, missile warning systems, flame detection, civil systems, and partial discharge detection [1–4]. For example, as indicated in a previous report, humans can realize partial discharge in the early stages to prevent unexpected damage owing to UV detection [5]. Thus, UV radiation leakage from artificial sources and insulation defects in high-voltage apparatus can be detected by analyzing the recorded electrical signals from UV PDs. Consequently, the design of a sensitive PD for detecting UV emissions or identifying UV overexposure in daily life has become desirable for commercial applications.

Typically, ideal UV PDs should fulfill the "5S" features: superb sensitivity, fast response speed, good regional selectivity, high signal-to-noise ratio (or extremely high on/off ratio), and excellent thermal and photostability (as well as superior reproducibility) [6–8]. As a result, one of the key elements is selecting an appropriate semiconductor material that is responsible for the photon-to-carrier convention. Zinc oxide (ZnO), which has unique physical and chemical properties, has become a well-known and environmentally friendly semiconductor owing to its wide direct bandgap ($E_g \approx 3.37$ eV), thermal stability, high electron mobility (166 $cm^2$/Vs), and high room-temperature excitonic binding energy (~60 meV) [9–11]. In particular, the synthesis roadmap for ZnO-based UV PDs comprises several methods, such as spin coating, dip coating, drop casting, spray pyrolysis, sputtering, atomic layer deposition (ALD), and chemical vapor deposition (CVD).

Thus, ZnO has proven to be a suitable semiconductor for manufacturing industrial UV PDs [12]. However, in several recent studies, self-powered ZnO-based UV PDs have exhibited slow response times (e.g., $t_{rise}/t_{fall}$: 2/32 s of ZnO@carbon dots/graphite; $t_{rise}/t_{fall}$: 0.5/0.45 s of ZnO/PVA; and $t_{rise}/t_{fall}$: <0.61/<0.61 s of Si/Te-doped ZnO@PMMA) and poor on/off ratios [13–15]. To address this problem, researchers have incorporated the piezoelectric effect in PDs to improve the response speed and further boost their photoresponsivity. Shen et al. recently applied an ex-situ piezoelectric effect to a p–i–n UV PD (ITO/PEDOT:PSS/TiO$_2$:P3HT/ZnO:PVDF/Al structure) [16]; they employed PVDF:ZnO as an electron transport layer (ETL) between the TiO$_2$:P3HT active layer and electrode in the device architecture. When the device was exposed to UV light, photogenerated electrons were driven from the TiO$_2$:P3HT to the ZnO:PVDF layer. The polarization of PVDF produces an internal electric field, thereby modulating the charge transport at the interface. Consequently, the on/off ratio of the self-powered PD was enhanced by 2.4 times under an applied voltage ($-10$ V poled). However, the recorded response time was slow (0.52/0.87 s). In another approach, by utilizing the intrinsic piezoelectricity of 2D-ZnO, Peng et al. fabricated a p–n UV PD using piezoelectric semiconductors (p-type GaN and n-type ZnO nanowires) as core materials [17]. Owing to the piezoelectric charges formed at two sides of the heterojunction interface under an external strain, which controls the separation, extraction, and recombination of photogenerated carriers, the PD exhibited a good on/off ratio (up to $7.36 \times 10^6$) and quick response time (6.9/6.4 ms). However, complicated methods (metal–organic CVD, electroplating process, laser lift-off process, coupled plasma etching technique, and radio-frequency magnetron sputtering), as well as costly metal electrodes (Au, Ni), have been used to fabricate PDs, which renders them expensive to produce and hinders their mass manufacturing. Therefore, the development of a self-powered UV PD that is both high-performing and cost-effective is a significant impetus for research.

Herein, we present a self-powered UV PD with a thin layer of poly [9,9-dioctylfluorene-co-N-[4-(3-methylpropyl)]-diphenylamine] (TFB) on a p-type and a thin film of ZnO@β-PVDF composite on an n-type. The performance of the ZnO-based sensor is enhanced under bias voltage via the in-situ piezoelectric effect, which occurs in the depletion region. In addition, our design considers a suitable structure without using costly metal electrodes (Ag, Au, etc.) and with simple solution processes at low temperatures. In summary, the UV PD that we successfully fabricated with the ITO/ZnO@PVDF/TFB/PEDOT:PSS structure exhibits a further on/off ratio—from $3.58 \times 10^3$ to $2.75 \times 10^4$—when poled with $-10$ V in one minute, a fast response speed (46/53 ms), and a high detectivity of $4.99 \times 10^{11}$ Jones when operated in the self-powered mode. In addition, the device exhibits over 1000 continuous on/off cycles and immensely durable photostability under UV irradiation.

## 2. Experimental Section

### 2.1. Materials

Zinc acetate dihydrate (Zn(CH$_3$COO)$_2$·2H$_2$O; ZA, 99.9%, Sigma-Aldrich, Seoul, Republic of Korea); polyvinylidene fluoride (PVDF; M$_w$ ≈ 534,000, Sigma-Aldrich, Seoul, Republic of Korea); poly(3,4-ethylenedioxythiophene)-poly(styrenesulfonate) (PEDOT:PSS; Orgacon™ dry re-dispersible pellets, Sigma-Aldrich, Seoul, Republic of Korea); poly [9,9-dioctylfluorene-co-N-[4-(3-methylpropyl)]-diphenylamine] (TFB; M$_w$ > 30,000, Sigma-Aldrich, Seoul, Republic of Korea); potassium hydroxide (KOH; 99.99%, Sigma-Aldrich, Seoul, Republic of Korea); dimethylacetamide (DMAc; anhydrous, 99.8%, Sigma-Aldrich, Seoul, Republic of Korea); 2-propanol (IPA; 99.5%, Sigma-Aldrich, Seoul, Republic of Korea), dimethyl sulfoxide (DMSO; anhydrous, ≥99.9%, Sigma-Aldrich, Seoul, Republic of Korea); methanol (CH$_3$OH; anhydrous, 99.8%, Sigma-Aldrich, Seoul, Republic of Korea); chlorobenzene (99.8%, Sigma-Aldrich, Seoul, Republic of Korea); ITO-coated PET substrate (sheet resistance of 14 Ω sq$^{-1}$, MTI Korea, Seoul, Republic of Korea).

## 2.2. Synthesis of ZnO Nanoparticles (ZnO NPs)

ZnO NPs were prepared through hydrolysis and condensation of ZA using KOH in a methanol solution at low temperature. Briefly, 2.46 g of ZA was dissolved in 125 mL of methanol in a beaker by heating at 60 °C. A clear solution was obtained by stirring the mixture at 500 rpm for 30 min. Subsequently, a base solution with 1.29 g of KOH dissolved in 65 mL of methanol was injected into the ZA hot solution. The mixture was then transferred to a sealed vial and stirred at 60 °C for 2 h. The white precipitates were separated from the milky-colored solution through centrifugation and washed three times with methanol to remove impurities. Finally, the as-obtained product was collected and dried in an oven at 50 °C.

## 2.3. Preparation of ZnO NPs@PVDF Nanocomposite

The PVDF powder was dissolved in DMAc at a concentration of 8 mg/mL through vigorous stirring at room temperature for 3 h. Next, 20 mg of as-synthesized ZnO NPs was dispersed in the solution through sonication in a bath for 30 min to obtain the ZnO NPs@PVDF suspension.

## 2.4. Fabrication of the Photodetector

The UV PD was fabricated in a p–n structure using a simple spin-coating process and low-temperature annealing. First, the pattern of the ITO-coated PET substrate (2 cm × 2 cm) was created using zinc powder and dilute HCl. The patterned substrate was then cleaned via ultrasonication for 10 min with acetone, IPA, ethanol, and deionized water. The ZnO NPs@PVDF suspension was then spin-coated onto the cleaned substrate at 2000 rpm for 30 s. The specimen was heat treated at 60 °C for 20 min on a hot plate, resulting in an n-type layer of ZnO@β-PVDF film. Subsequently, a p-type solution of TFB/chlorobenzene solution (10 mg/mL) was coated onto the n-type layer at 3000 rpm for 30 s, heated for 20 min at 60 °C, and then baked for 20 min at 60 °C. The top electrode was prepared by spin-coating 100 μL of PEDOT:PSS solution (1.3 wt % in IPA and DMSO) on the surface of the p-type layer at 1000 rpm for 60 s and heated at 60 °C for 30 min. The active area of the UV PD was determined to be 0.7 cm$^2$ based on the overlap region of the ITO and PEDOT:PSS. The fabrication process of the UV PD is shown schematically in Figure 1.
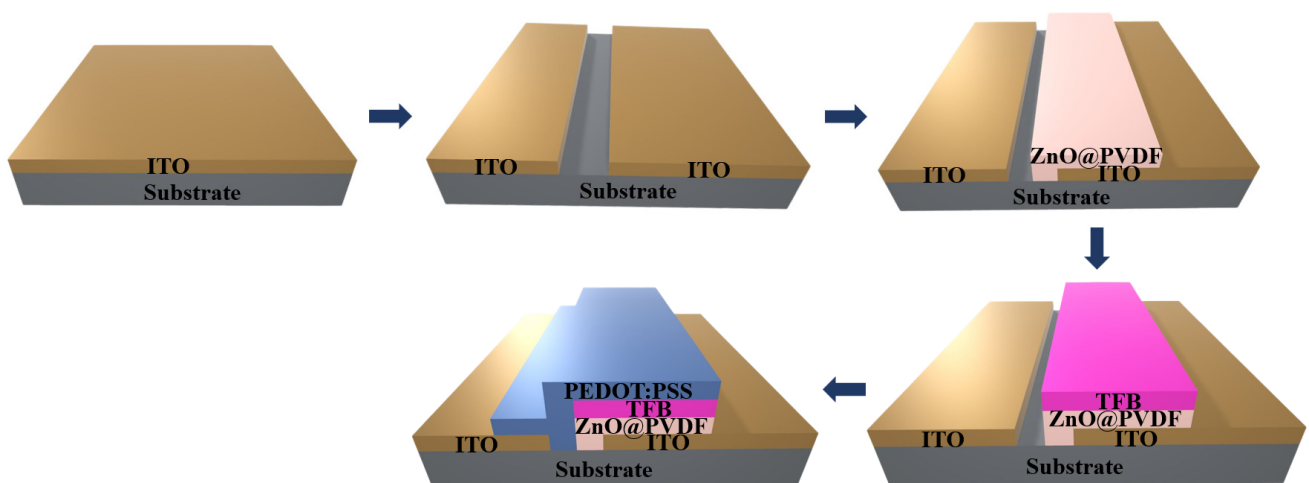


**Figure 1.** Fabrication process of a self-powered ZnO NPs@β-PVDF-based PD.

## 2.5. Analysis and Measurement

XRD (Rigaku DMAX 2200, Tokyo, Japan) employing Cu Kα radiation (λ = 1.5406 Å) at a scan rate of 2° min$^{-1}$ was used to confirm the formation of ZnO NPs. Grazing incidence XRD (GIXRD; Rigaku DMAX 2200, Tokyo, Japan) was used to confirm the formation of β-PVDF and ZnO@β-PVDF films. FTIR (Bruker Vertex 70, Ettlingen, Germany) was used

to determine the functional groups of ZnO NPs and β-PVDF. SEM (Hitachi S-4700, Tokyo, Japan) was used to examine the surface morphology and elemental distribution of ZnO NPs. A focused ion beam SEM (FEI Nova Nanolab 200,Thermo Fisher, MA, USA) was used to obtain a cross-sectional image of the complete structure of the UV PD. A UV–visible spectroscopy instrument (UV–vis; Agilent 8453, Santa Clara, CA, USA) was used to perform optical characterization of the device. The spectral response of the UV PD was measured using an analyzer (Keithley 2400 SourceMeter, Cleveland, OH, USA) under a UV lamp (VL6.LC, Vilber Lourmat, Marne-la-Vallée, France) with a wavelength of 365 nm, which served as the light source.

### 3. Results and Discussion

To analyze the crystalline structure of the substance and phase of the polymer, Figure 2a presents the X-ray diffraction (XRD) patterns of the ZnO nanoparticles (NPs) and β-PVDF and ZnO@β-PVDF thin films. The diffraction peaks located at 31.7°, 34.33°, 36.15°, 47.42°, and 56.47° corresponded to the (100), (002), (101), (102), and (110) crystal planes of ZnO (JCPDS card no. 01-080-0075), respectively. The characteristic peak of the polymer film appeared at 20.4°, corresponding to the (110) reflection of the β phase in PVDF. Despite having a broad peak, the center located at 20.4° confirmed the dominance of β-PVDF over α-PVDF, which agrees with previous reports [18–20]. In addition, Figure 2b depicts the Fourier-transform infrared (FTIR) spectra of the as-prepared ZnO NPs and ZnO@β-PVDF thin films in the range of 1400 to 500 cm$^{-1}$. The two prominent peaks at 438 and 840 cm$^{-1}$ observed in the ZnO@β-PVDF were the vibrations of the Zn–O stretching and $CH_2$ rocking of the β-phase PVDF, respectively [21–23]. Hence, a thin layer of the ZnO@β-PVDF nanocomposite was successfully prepared using a facile spin-coating process at a low temperature of 60 °C. The optical properties of the ZnO@β-PVDF thin film were observed using the UV–vis spectrum. As shown in Figure 2c, ZnO fillers have strong UV absorption, indicating that they would be effective photo-absorbers for fabricating UV PDs. Furthermore, Figure S1 shows the effect of PVDF mixing on the optical absorption. Owing to its excellent transparency (over 97.7%) in the wavelength range of 250–800 nm, PVDF is a suitable matrix material for UV-PD-based nanocomposites. The optical bandgap of the ZnO core material was estimated to be 3.3 eV, according to the Tauc plot (inset in Figure 2c). This was consistent with the previously reported values [24].

The synthesized ZnO NPs appeared to be spherical in shape with a diameter below 20 nm, as shown in the scanning electron microscopy (SEM) image (Figure S2). Figure 3a shows the surface morphology of the ZnO@β-PVDF thin film. ZnO NPs can form tight and extremely close contacts to form a dense and continuous layer. In particular, β-PVDF might fill pinholes and voids, which are commonly present in films spin-coated with NP solutions, resulting in the effective separation of the top and bottom electrodes of UV PDs and a reduction in the charge leakage. Additionally, the energy dispersive X-ray (EDX) mapping images depicted a uniform distribution of Zn and O with a Zn:O ratio (at.%) of 45.99:54.01, indicating the O-rich composition of the ZnO NPs [25]. The complete architecture of the fabricated UV PD is shown in Figure 3b. The layer thicknesses of the components were determined from the cross-sectional SEM images (see Figure 3c). In this study, the UV PD was constructed in a vertical configuration with a bottom electrode of ITO (100 nm), a layer of n-type ZnO@-PVDF (30 nm) serving as the electron transport layer, a very thin layer of p-type TFB functioning as the hole transport layer, and a top electrode of PEDOT:PSS (33 nm). The operating mechanism of the prepared p–n UV PD is shown in Figure 3d,e. Figure 3d shows the conduction band (CB), valence band (VB), and work function (WF) of the constituent materials before the contact [26–29]. When a contact between n-type ZnO and p-type TFB is formed, the charge carriers flow until the Fermi levels align. Consequently, a depletion area is established at the interface of the p–n junction. The difference between the WFs of the p-type and n-type creates a built-in potential ($V_{bi}$), which facilitates the separation of photogenerated carriers. When the device is exposed to UV light, the UV radiation penetrates the depletion layer, generating electrons

and holes. The excited charge carriers are separated by $V_{bi}$ and driven by band alignment to suitable electrodes (Figure 3e). Notably, n-type ZnO is combined with β-PVDF, resulting in a β-PVDF-induced electric field in the in-situ depletion region, boosting the photogenerated electrons to the ITO electrode.
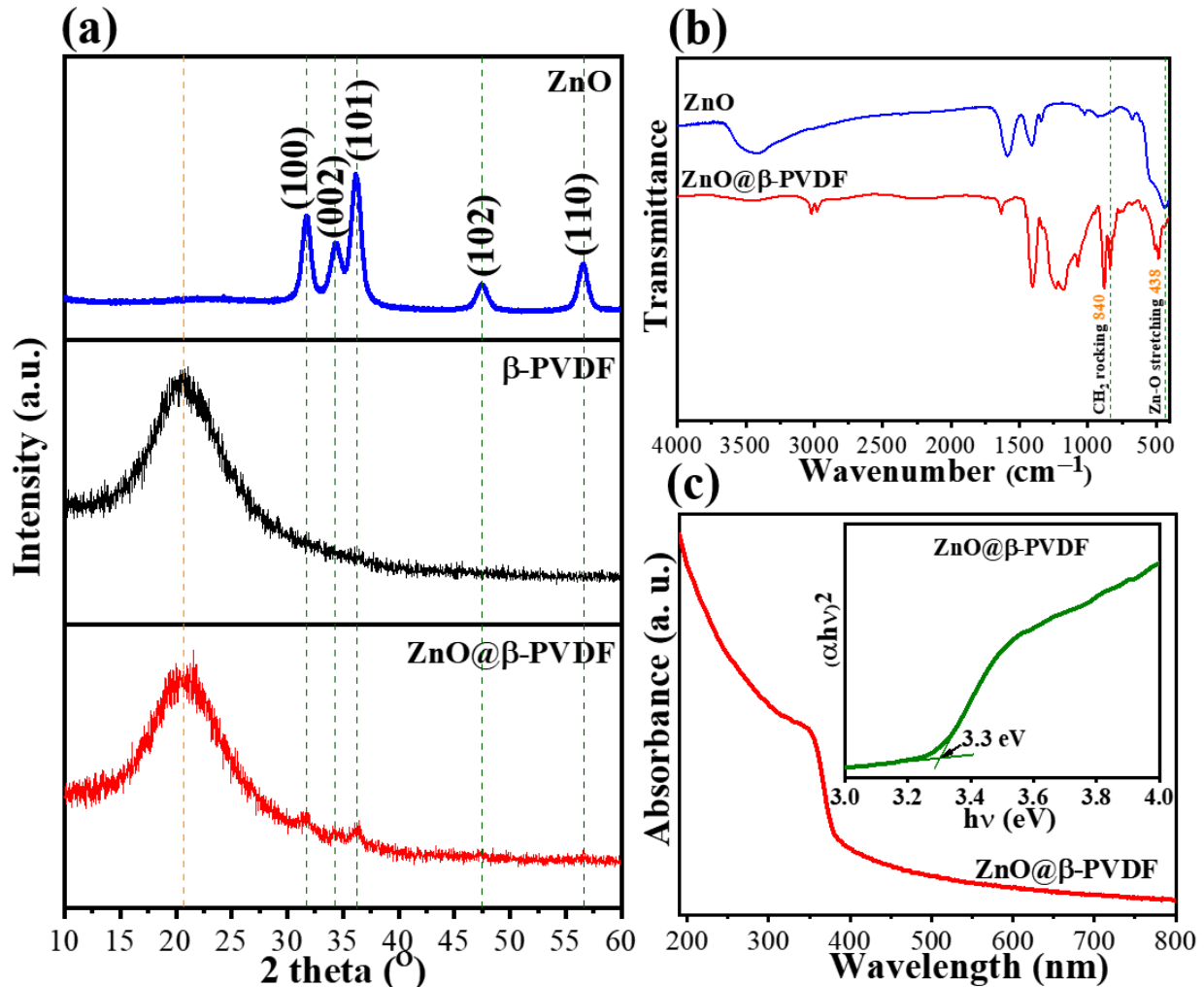


**Figure 2.** (**a**) X-ray diffraction patterns of ZnO NPs and β-PVDF and ZnO@β-PVDF thin films; (**b**) Fourier-transform infrared spectra of ZnO NPs and the ZnO@β-PVDF thin film; (**c**) UV–vis absorbance spectrum (inset shows Tauc plot) of the ZnO@β-PVDF thin film.

To evaluate the performance of the as-prepared UV PD, Figure 4a–d show the basic characteristic plots of the device under zero bias. Accordingly, Figure 4a shows the logarithmic I–V curves of the device, recorded in the dark and under 365-nm UV lamp irradiation. We observed that the fabricated PD could operate in the self-power mode and exhibited a low dark current of $6.35 \times 10^{-10}$ A. The achieved value was the result of the support of the PVDF, which prevented pinholes and voids in the n-type layer. Figure 4b depicts the relationship between the photoresponse and incoming light intensity, which ranged between 0.35 and 1.22 mW/cm$^2$. Owing to the increase in the quantity of photogenerated electrons and holes under high-intensity 365-nm UV irradiation, the self-powered UV PD exhibited an increase in photocurrent from $7 \times 10^{-7}$ to $2.27 \times 10^{-6}$ A. Therefore, the produced on/off ratio of the UV PD increased from $1.1 \times 10^3$ to $3.58 \times 10^3$. A simple power law can be employed to simulate the relationship between the generated photocurrent and the incident light intensity: $J_{photo} \propto P_{opt}{}^\theta$, where θ is the index of the power exponent. The non-unity exponent (θ = 0.94) in Figure 4c indicates the presence of trap states and defects in the core material [30–32]. Two essential PD figure-of-merit characteristics are

the responsivity (R) and specific detectivity (D*), which are described in the following equations [33,34]:

$$R = \frac{J_{photo}}{P_{opt}} \tag{1}$$

$$D^* = \frac{R}{\sqrt{2qJ_{dark}}} \tag{2}$$

where $J_{photo}$ ($J_{photo} = J_{light} - J_{dark}$) and $J_{dark}$ are the output photocurrent densities under 365-nm UV illumination and the dark current density, respectively, $P_{opt}$ is the incident optical power, and q is the charge of an electron. According to the simple power law and Equation (1), the relationship between R and the photocurrent is $R \propto P_{opt}^{\theta-1}$. Hence, parameters R and D* are dependent on $P_{opt}$ when $\theta < 1$. As shown in Figure 4d, they tended to decrease with the increase in intensity. The rise and fall times ($t_{rise}/t_{fall}$) are used to describe the response speed, which reflects how rapidly the PD responds to an optical signal. Here, $t_{rise}$ and $t_{fall}$ measure the amount of time required for a response to move from 10% to 90% and decrease from 90% to 10% of the maximum value, respectively [35]. The prepared PD exhibited a rapid switching time of 45/46 ms at a light intensity of 0.89 mW/cm² (Figure 4e). This response time was superior to that of previously reported ZnO-based UV PDs (Table 1).

**Table 1.** Performance comparisons between the as-prepared PD and previously reported ZnO-based PDs.

| Photodetector | Device Structure | Structure/ Role of ZnO (Thickness) | Device Fabrication Technique | Bias (V) | D (Jones) | Rise/Fall Time | On/Off Ratio | Ref. |
|---|---|---|---|---|---|---|---|---|
| ITO/ZnO@PVDF/ TFB/PEDOT:PSS | P–N | nanoparticles/ n-type layer (~30 nm) | spin-coating | 0 | $1.676 \times 10^{11}$ | 45/46 ms | $3.58 \times 10^3$ | This work |
| ITO/ZnO@PVDF/ TFB/PEDOT:PSS (−10 V poled) | | | | 0 | $4.994 \times 10^{11}$ | 46/53 ms | $2.75 \times 10^4$ | This work |
| In/BaTiO₃-ZnO bilayer/In | M–S–M | nanoparticles/ active layer (78 nm) | spin-coating | 3 | $2.7 \times 10^{11}$ | 0.11/5.8 ms | $1.43 \times 10^4$ | [36] |
| In/ZnO MW@polyaniline/In | M–S–M | microwire/ active layer | CVD | −1 | $2 \times 10^{11}$ | 0.44/0.42 s | | [37] |
| Graphene/ZnO | Metal– Semiconductor | nanoparticles/ active layer | direct writing | 1 | $1.2 \times 10^7$ | 8.76/18.13 s | $1.729 \times 10^3$ | [38] |
| Graphite/ZnO@ carbon dots | Metal– Semiconductor | nanorods/ active layer | dip-coating | 0 | $4.27 \times 10^8$ | 2/32 s | 1.1 | [13] |
| ITO/ZnO:GQD/Poly-TPD/Ag | P–N | nanoparticles/ n-type layer (100 nm) | spin-coating | −3 | $2.1 \times 10^{11}$ | 0.37/0.78 s | 12 | [27] |
| ITO/ZnO/PEDOT: PSS/Ag | P–N | textured grains/ n-type layer | spray pyrolysis | −3 | $1.27 \times 10^{11}$ | 0.7/2.95 s | | [39] |
| ITO/PMMA/5 wt % ZnO/Ag ITO/PS/5 wt % ZnO/Ag ITO/PVDF-TrFE/5 wt % ZnO/Ag | M–S–M | nanoparticles/ active layer (680 nm) | spin-coating | 2 | $1.02 \times 10^{11}$ $1.89 \times 10^{12}$ $2.27 \times 10^{13}$ | 14.57/45.69 s 12.36/10.18 s 9.37/6.91 s | $2.5 \times 10^2$ $2.2 \times 10^3$ $1.43 \times 10^4$ | [40] |
| P-Si/SiO₂/ZnO/ PVA/Ag | P–N | nanoparticles/ n-type layer | spin-coating | 0 | $4.6 \times 10^{10}$ | 0.5/0.45 s | | [14] |
| graphene@Au wire/ZnO/GaN/Si/ CNT@Au wire | P–N | nanosheets/ n-type layer | hydride vapor phase epitaxy and hydrother-mal process | 0 | $4.25 \times 10^{10}$ | 0.1 s | | [41] |
| ITO/Fe-doped ZnO/BiVO₄ | N–N het-erostructure | thin film/ n-type layer (200 nm) | spin-coating and drop casting | 0.1 | $3.66 \times 10^9$ | 0.17/0.17 s | | [42] |

**Table 1.** *Cont.*

| Photodetector | Device Structure | Structure/ Role of ZnO (Thickness) | Device Fabrication Technique | Bias (V) | D (Jones) | Rise/Fall Time | On/Off Ratio | Ref. |
|---|---|---|---|---|---|---|---|---|
| InGa/Si/Te-doped ZnO@PMMA/Au | P–N | nanorods/ n-type layer | CVD | 0 | $1.1 \times 10^{12}$ | <0.61/<0.61 s | 275 | [15] |
| Si/SiO$_2$/ZnO/CuI/ Au/Ag | P–N heterostructure | thin film/ n-type layer (150 nm) | ALD and sputtering | 0 | $1.7 \times 10^{10}$ | 0.41/0.08 s | 4250 | [43] |
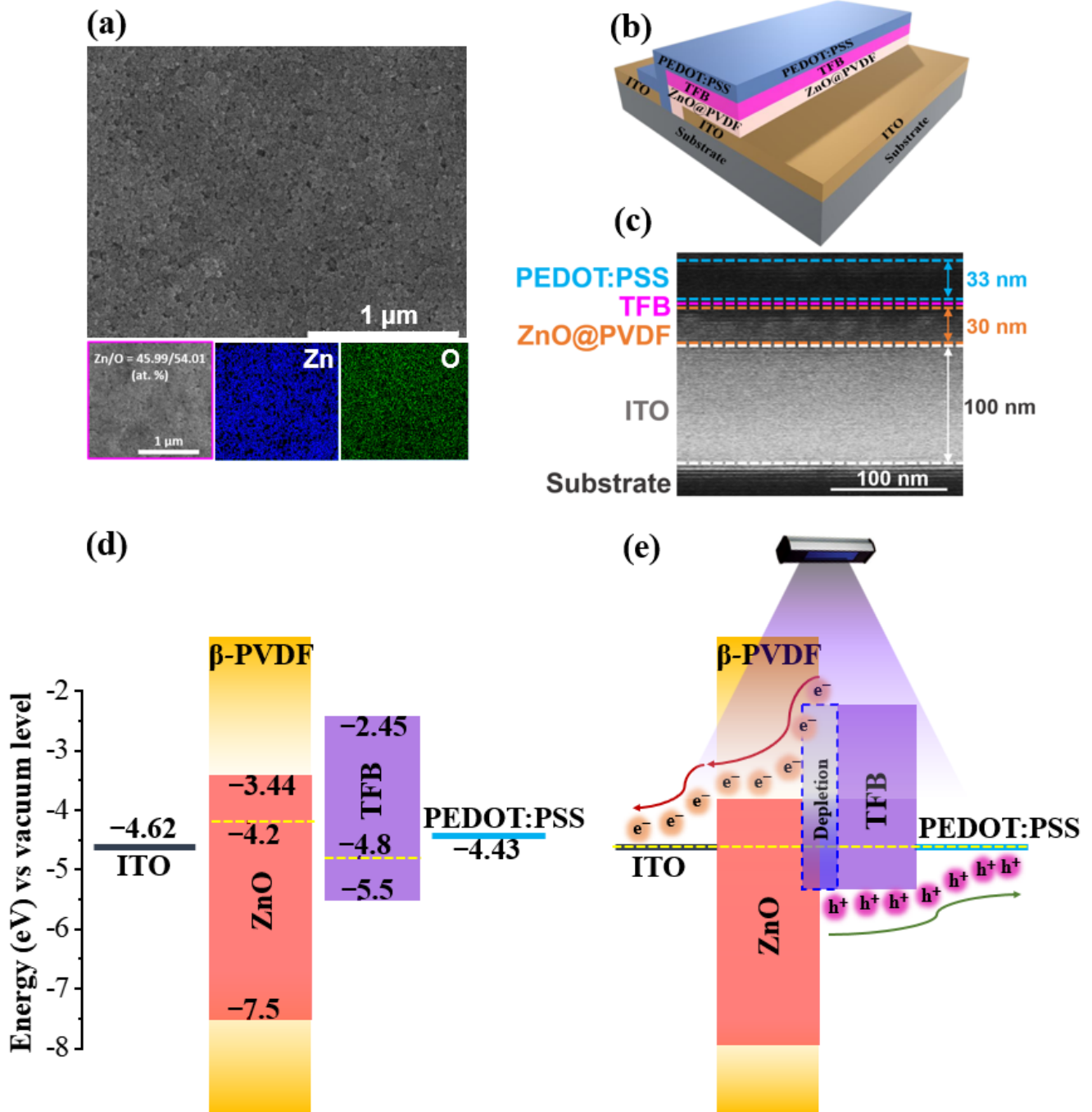
**Figure 3.** (**a**) SEM image and EDX mapping images of ZnO@β-PVDF thin film; (**b**) A complete device structure; (**c**) Cross-section image of the prepared device. The operating mechanism of the PD (**d**) before contact and (**e**) under UV light.
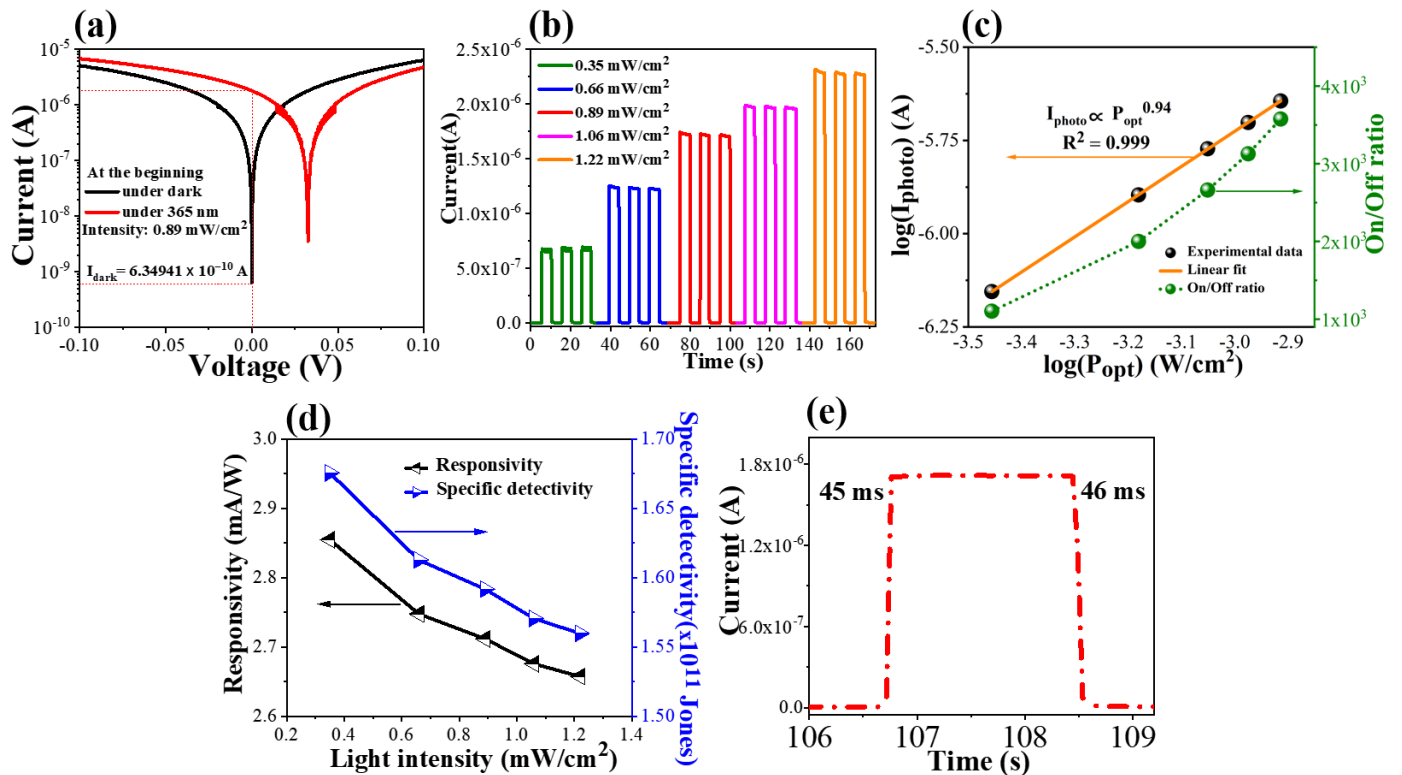
**Figure 4.** Performance of the self-powered PD without poled voltage: (**a**) Logarithmic I–V curves of the PD under dark and under light; (**b**) I–t plots under various light intensities; (**c**) logarithm of photocurrent and on/off ratio as a function of power; (**d**) R and D* of the PD as functions of different light intensities; (**e**) rise and fall times of the PD.

Regarding the effect of the PVDF-induced internal electric field on the UV PD's performance, the photoresponses of the self-powered PD under forward bias (FW) and reverse bias (RV) are shown in Figure S3. In more detail, a voltage was applied to the UV PD within a minute using a DC machine to create the polarization of β-PVDF in the depletion region. Thereafter, the I−t curves were recorded at 0 V under a light intensity of 0.89 mW/cm$^2$ from a 365 nm-UV lamp. The values for the dark currents and photocurrents were then extracted and are presented in Figure 5a. The photocurrent improved considerably, while the dark current changed dramatically under bias. The mechanism for the reduction in the dark current is depicted in Figure 5b–d. Briefly, when the components of the PD were in contact, electrons were injected from the PEDOT:PSS electrode to the ITO electrode through traps in the photoactive region, producing a dark current. After the ZnO@β-PVDF was polarized through reverse biases, an in-situ internal electric field was formed in the depletion region (Figure 5c). This electric field prevented the injection of electrons from PEDOT:PSS to ITO, resulting in a decline in the dark current. In contrast, after the ZnO@β-PVDF was polarized through forward biases, the electron injection was facilitated by a favorable internal electric field, resulting in an increased dark current (Figure 5d). Therefore, a reverse bias was selected to enhance the performance of the prepared UV PD, and the results are depicted in Figure 6.
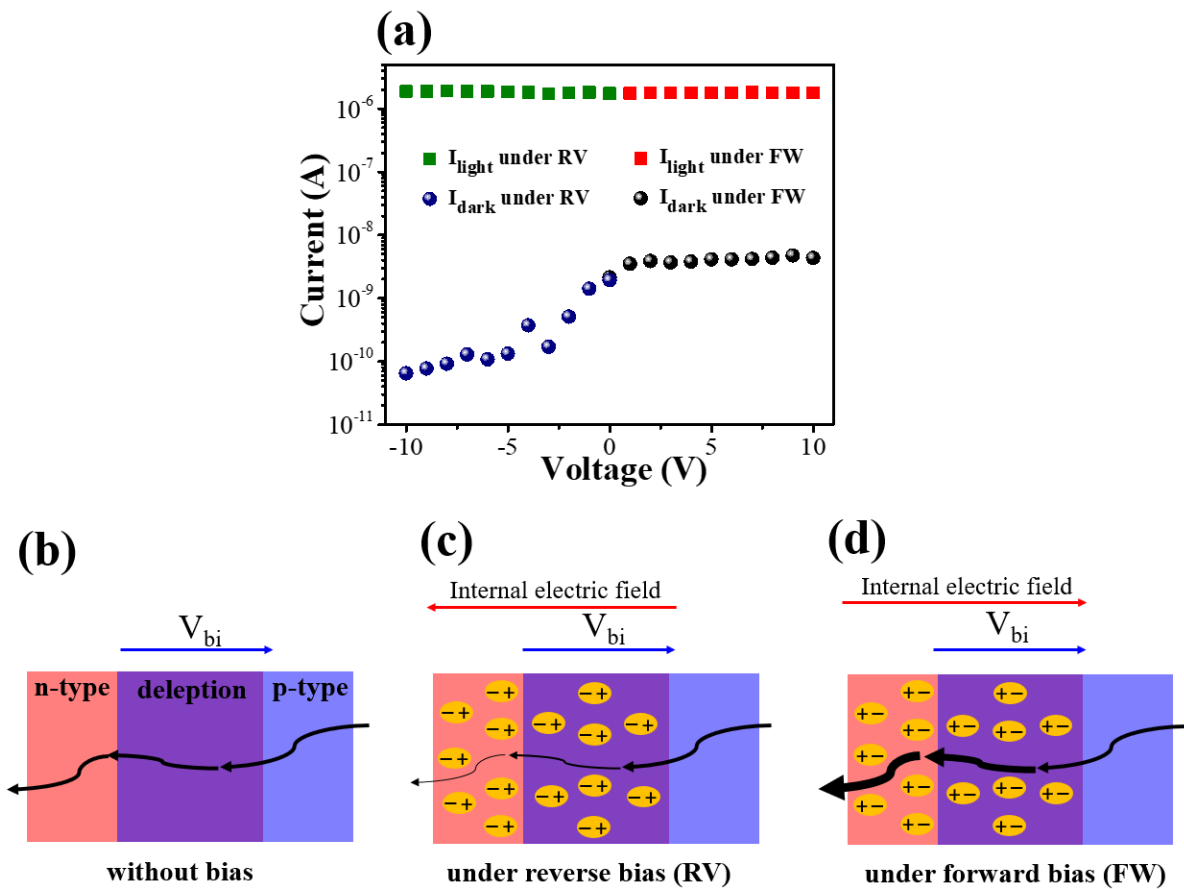
**Figure 5.** (**a**) Photocurrent and dark current of the self-powered PD under various reverse biases and forwards biases. The dark current of the PD (**b**) without bias, (**c**) with reverse biases, and (**d**) with forward biases.

Figure 6 shows the photoelectronic performance of the self-powered UV PD after poling with an applied reverse voltage of $-10$ V. We observed that the in-situ piezoelectric effect of β-PVDF enhanced the UV PD's performance. Remarkably, the dark current at zero bias decreased by $9.82 \times 10^{-11}$ A under a reverse bias (Figure 6a) compared with the value at which voltage poling was not present ($6.35 \times 10^{-10}$ A, in Figure 4a). Furthermore, when the incidence intensity varied between 0.35 and 1.22 mW/cm$^2$, the generated current also improved slightly, increasing from $8.2 \times 10^{-7}$ to $2.7 \times 10^{-6}$ A (Figure 6b). When the dark current decreased significantly, the UV on/off ratio reached $2.75 \times 10^4$ at a light intensity of 0.89 mW/cm$^2$ and was enhanced 7.68 times compared with no poling. In addition, the R and D values and response time of the self-powered UV PD improved to values as high as $2.75 \times 10^4$, 3.35 mW/A, $4.99 \times 10^{11}$ Jones, and 46/53 ms ($t_{rise}/t_{fall}$) at the illumination of a 365 nm UV lamp, respectively (Figure 6c–e).

To assess the repeatability and photostability of the as-fabricated UV PD, Figure 7a,b depict the photoresponse of the self-powered device under 365 nm illumination with a power density of 0.89 mW/cm$^2$. Accordingly, Figure 7a shows that the generated current remained constant for 1000 subsequent on/off cycles. In addition to displaying consistency throughout multiple cycles, the UV PD exhibited outstanding stability under continuous UV light for 1000 s in the ambient environment (Figure 7b). In addition, the ZnO@β-PVDF nanocomposite-based UV PD developed in this study had characteristics that were greater than those of the ZnO-based PDs described in previous publications (see Table 1). Owing to its remarkable long-term stability and high detectivity, the prepared UV PD is a promising candidate for UV photodetection in practical applications.
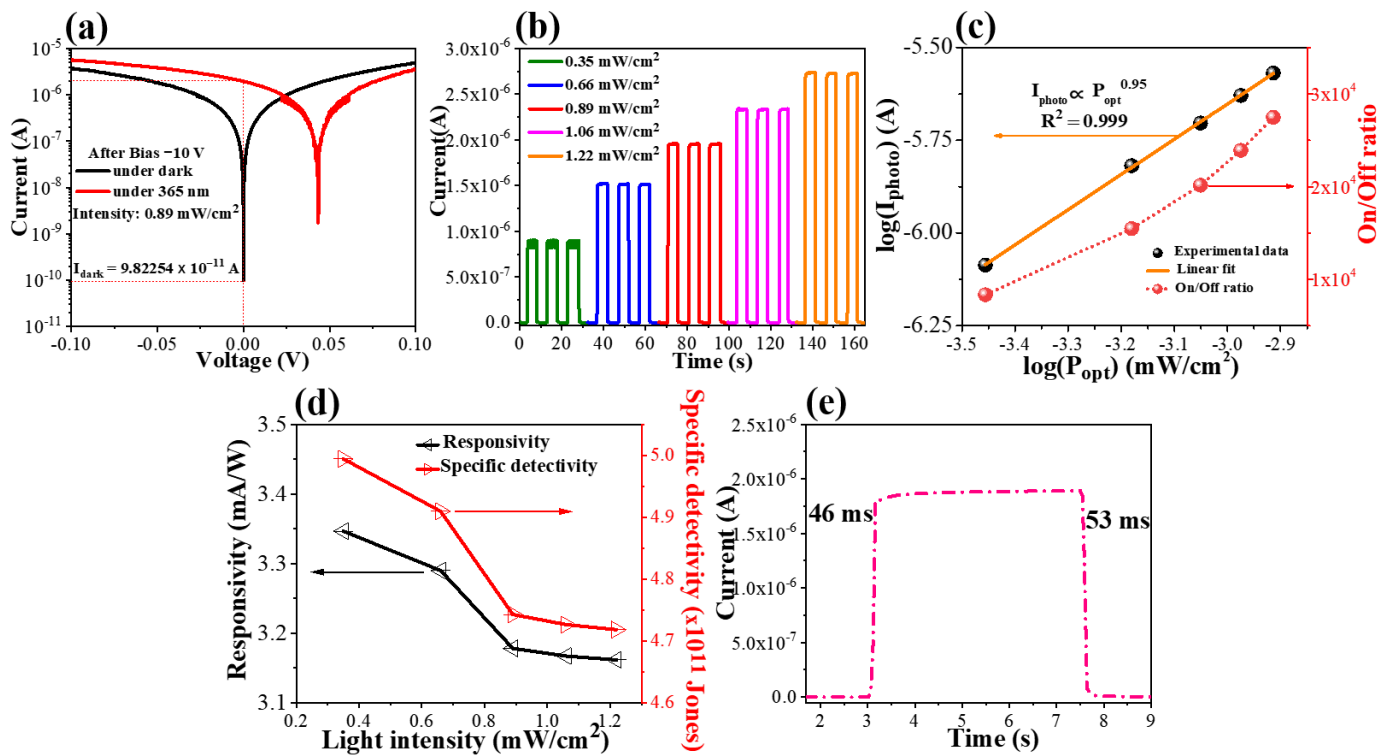
**Figure 6.** Performance of the self-powered PD with a poled voltage of -10 V: (**a**) Logarithmic I–V curves of the PD under dark and light; (**b**) I–t plots under various UV intensities; (**c**) logarithm of photocurrent and on/off ratio as a function of power; (**d**) R and D* of PD as functions of different light intensities; (**e**) rise and fall times of the PD.
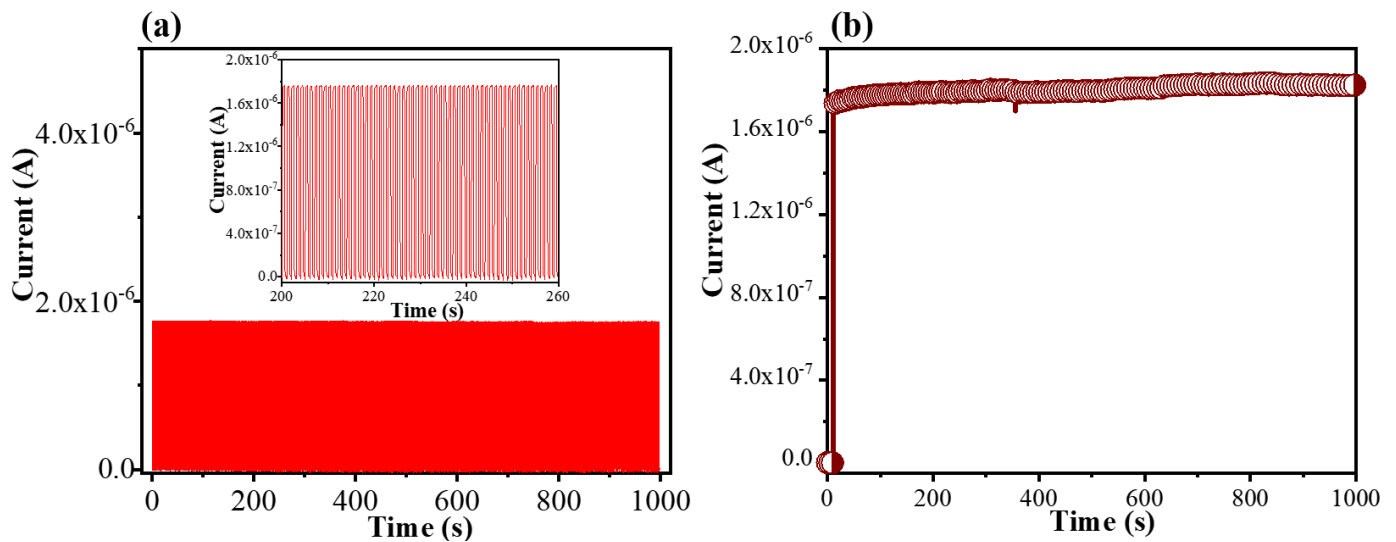


**Figure 7.** (**a**) Reproducibility (inset shows high magnification of stable photoresponse) and (**b**) photostability of the self-powered device for 1000 on/off switching cycles with a remaining time of 1000 s.

## 4. Conclusions

We successfully fabricated an efficient UV PD based on n-ZnO@β-PVDF/p-TFB using a simple spin-coating process at 60 °C. The UV PD demonstrated good photoresponse characteristics to 365 nm UV light with zero bias. The device performance can be significantly boosted owing to the in-situ piezoelectric effect of β-PVDF occurring in the depletion region.

The self-powered PD exhibited a high specific detectivity (D = 4.99 × $10^{11}$ Jones), excellent on/off ratio of 2.75 × $10^4$, and fast response speed of 46/53 ms ($t_{rise}$/$t_{fall}$). Furthermore, the as-prepared PD exhibited outstanding photoresponse stability under continuous UV illumination, along with good reproducibility over 1000 consecutive on/off cycles. Our findings suggest a new approach for developing a cost-effective UV PD for optoelectronic applications in the relevant fields.

**Supplementary Materials:** The following supporting information can be downloaded at: https://www.mdpi.com/article/10.3390/coatings13050921/s1, Figure S1. The transmittance spectra of 30 nm-thick β-PVDF, ZnO, and ZnO@β-PVDF samples. Figure S2. SEM image of ZnO nanoparticles loaded on a glass substrate (on the left) and an individual ZnO particle (on the right). Figure S3. Logarithmic I−t curves of the photodetector under (a) reverse bias and (b) forward bias.

**Author Contributions:** Conceptualization, T.M.H.N.; Methodology, T.M.H.N.; Validation, C.W.B.; Investigation, T.M.H.N.; Writing—original draft, T.M.H.N.; Writing—review & editing, C.W.B.; Supervision, C.W.B.; Funding acquisition, C.W.B. All authors have read and agreed to the published version of the manuscript.

**Institutional Review Board Statement:** Not applicable.

**Informed Consent Statement:** Not applicable.

**Data Availability Statement:** Not applicable.

**Conflicts of Interest:** The authors declare no conflict of interest.

## References

1. Kang, C.H.; Dursun, I.; Liu, G.; Sinatra, L.; Sun, X.; Kong, M.; Pan, J.; Maity, P.; Ooi, E.-N.; Ng, T.K. High-speed colour-converting photodetector with all-inorganic CsPbBr$_3$ perovskite nanocrystals for ultraviolet light communication. *Light Sci. Appl.* **2019**, *8*, 1–12.
2. Ye, Q.; Zhang, X.; Yao, R.; Luo, D.; Liu, X.; Zou, W.; Guo, C.; Xu, Z.; Ning, H.; Peng, J. Research and progress of transparent, flexible tin oxide ultraviolet photodetector. *Crystals* **2021**, *11*, 1479. [CrossRef]
3. Zhang, Z.; Zheng, W.; Lin, R.; Huang, F. High-sensitive and fast response to 255 nm deep-UV light of CH$_3$NH$_3$PbX$_3$ (X = Cl, Br, I) bulk crystals. *Royal Soc. Open Sci.* **2018**, *5*, 180905. [CrossRef] [PubMed]
4. Sheng, X.; Yu, C.; Malyarchuk, V.; Lee, Y.H.; Kim, S.; Kim, T.; Shen, L.; Horng, C.; Lutz, J.; Giebink, N.C. Silicon-Based Visible-Blind Ultraviolet Detection and Imaging Using Down-Shifting Luminophores. *Adv. Opt. Mater.* **2014**, *2*, 314–319. [CrossRef]
5. Nguyen, T.M.H.; Lee, S.K.; Kim, S.; Bark, C.W. Practical Demonstration of Deep-Ultraviolet Detection with Wearable and Self-Powered Halide Perovskite-Based Photodetector. *ACS Appl. Mater. Interfaces* **2021**, *13*, 57609–57618. [CrossRef]
6. Sang, L.; Liao, M.; Sumiya, M. A comprehensive review of semiconductor ultraviolet photodetectors: From thin film to one-dimensional nanostructures. *Sensors* **2013**, *13*, 10482–10518. [CrossRef]
7. Zhang, Y.; Song, W. High performance self-powered CuZnS/GaN UV photodetectors with ultrahigh on/off ratio (3× $10^8$). *J. Mater. Chem. C* **2021**, *9*, 4799–4807. [CrossRef]
8. Nguyen, T.M.H.; Shin, S.G.; Choi, H.W.; Bark, C.W. Recent advances in self-powered and flexible UVC photodetectors. *Exploration* **2022**, *2*, 20210078. [CrossRef]
9. Khokhra, R.; Bharti, B.; Lee, H.-N.; Kumar, R. Visible and UV photo-detection in ZnO nanostructured thin films via simple tuning of solution method. *Sci. Rep.* **2017**, *7*, 1–14.
10. Kamarulzaman, N.; Kasim, M.F.; Rusdi, R. Band gap narrowing and widening of ZnO nanostructures and doped materials. *Nanoscale Res. Lett.* **2015**, *10*, 1–12. [CrossRef]
11. Zhang, H.; Jia, Z. Application of porous silicon microcavity to enhance photoluminescence of ZnO/PS nanocomposites in UV light emission. *Optik* **2017**, *130*, 1183–1190. [CrossRef]
12. Wang, H.-C.; Hong, Y.; Chen, Z.; Lao, C.; Lu, Y.; Yang, Z.; Zhu, Y.; Liu, X. ZnO UV photodetectors modified by Ag nanoparticles using all-inkjet-printing. *Nanoscale Res. Lett.* **2020**, *15*, 1–8. [CrossRef] [PubMed]
13. Sinha, R.; Roy, N.; Mandal, T.K. Growth of carbon dot-decorated ZnO nanorods on a graphite-coated paper substrate to fabricate a flexible and self-powered schottky diode for UV detection. *ACS Appl. Mater. Interfaces* **2020**, *12*, 33428–33438. [CrossRef] [PubMed]

14. Mousavi, S.S.; Sajad, B. Self-powered Vs. high speed ZnO-based photodetectors. *Mater. Res. Bull.* **2022**, *155*, 111950. [CrossRef]

15. Liu, Y.; Song, Z.; Hu, M.; Chen, J.; Yuan, S.; Xu, L. Self-powered adjustable UV and NIR photodetectors based on one-step synthesized $TeO_2$ doped ZnO composite nanorods/Si heterojunction. *Sens. Actuator A Phys.* **2021**, *331*, 113009. [CrossRef]

16. Shen, T.L.; Chu, Y.W.; Liao, Y.K.; Lee, W.Y.; Kuo, H.C.; Lin, T.Y.; Chen, Y.F. Ultrahigh-performance self-powered flexible photodetector driven from photogating, piezo-phototronic, and ferroelectric effects. *Adv. Opt. Mater.* **2020**, *8*, 1901334. [CrossRef]

17. Peng, Y.; Lu, J.; Wang, X.; Ma, W.; Que, M.; Chen, Q.; Li, F.; Liu, X.; Gao, W.; Pan, C. Self-powered high-performance flexible GaN/ZnO heterostructure UV photodetectors with piezo-phototronic effect enhanced photoresponse. *Nano Energy* **2022**, *94*, 106945. [CrossRef]

18. Mahadeva, S.K.; Berring, J.; Walus, K.; Stoeber, B. Effect of poling time and grid voltage on phase transition and piezoelectricity of poly (vinyledene fluoride) thin films using corona poling. *J. Phys. D Appl. Phys.* **2013**, *46*, 285305. [CrossRef]

19. Jin, Z.; Lei, D.; Wang, Y.; Wu, L.; Hu, N. Influences of poling temperature and elongation ratio on PVDF-HFP piezoelectric films. *Nanotechnol. Rev.* **2021**, *10*, 1009–1017. [CrossRef]

20. Gregorio, R., Jr.; de Souza Nociti, N.C.P. Effect of PMMA addition on the solution crystallization of the alpha and beta phases of poly (vinylidene fluoride) (PVDF). *J. Phys. D Appl. Phys.* **1995**, *28*, 432. [CrossRef]

21. Cai, X.; Lei, T.; Sun, D.; Lin, L. A critical analysis of the α, β and γ phases in poly (vinylidene fluoride) using FTIR. *RSC Adv.* **2017**, *7*, 15382–15389. [CrossRef]

22. Mohammadi, B.; Yousefi, A.A.; Bellah, S.M. Effect of tensile strain rate and elongation on crystalline structure and piezoelectric properties of PVDF thin films. *Polym. Test.* **2007**, *26*, 42–50. [CrossRef]

23. Devi, P.G.; Velu, A.S. Synthesis, structural and optical properties of pure ZnO and Co doped ZnO nanoparticles prepared by the co-precipitation method. *J. Theor. Appl. Phys.* **2016**, *10*, 233–240. [CrossRef]

24. Lee, W.; Yeop, J.; Heo, J.; Yoon, Y.J.; Park, S.Y.; Jeong, J.; Shin, Y.S.; Kim, J.W.; An, N.G.; Kim, D.S. High colloidal stability ZnO nanoparticles independent on solvent polarity and their application in polymer solar cells. *Sci. Rep.* **2020**, *10*, 1–10.

25. Sahai, A.; Goswami, N. Structural and optical investigations of oxygen defects in zinc oxide nanoparticles. *N. AIP Conf. Proc.* **2015**, *1665*, 050023.

26. Zhou, Y.; Fuentes-Hernandez, C.; Shim, J.; Meyer, J.; Giordano, A.J.; Li, H.; Winget, P.; Papadopoulos, T.; Cheun, H.; Kim, J. A universal method to produce low–work function electrodes for organic electronics. *Science* **2012**, *336*, 327–332. [CrossRef]

27. Tran, M.H.; Park, T.; Hur, J. Solution-processed ZnO: Graphene quantum dot/Poly-TPD heterojunction for high-performance UV photodetectors. *Appl. Surf. Sci.* **2021**, *539*, 148222. [CrossRef]

28. Hwang, J.; Kim, E.-G.; Liu, J.; Bredas, J.-L.; Duggal, A.; Kahn, A. Photoelectron spectroscopic study of the electronic band structure of polyfluorene and fluorene-arylamine copolymers at interfaces. *J. Phys. Chem. C* **2007**, *111*, 1378–1384. [CrossRef]

29. Zhang, W.; Bi, X.; Zhao, X.; Zhao, Z.; Zhu, J.; Dai, S.; Lu, Y.; Yang, S. Isopropanol-treated PEDOT: PSS as electron transport layer in polymer solar cells. *Org. Electron.* **2014**, *15*, 3445–3451. [CrossRef]

30. Zeng, L.H.; Chen, Q.M.; Zhang, Z.X.; Wu, D.; Yuan, H.; Li, Y.Y.; Qarony, W.; Lau, S.P.; Luo, L.B.; Tsang, Y.H. Multilayered $PdSe_2$/perovskite Schottky junction for fast, self-powered, polarization-sensitive, broadband photodetectors, and image sensor application. *Adv. Sci.* **2019**, *6*, 1901134. [CrossRef]

31. Fang, H.; Hu, W. Photogating in low dimensional photodetectors. *Adv. Sci.* **2017**, *4*, 1700323. [CrossRef] [PubMed]

32. Zhang, T.; Wang, F.; Zhang, P.; Wang, Y.; Chen, H.; Li, J.; Wu, J.; Chen, L.; Chen, Z.D.; Li, S. Low-temperature processed inorganic perovskites for flexible detectors with a broadband photoresponse. *Nanoscale* **2019**, *11*, 2871–2877. [CrossRef]

33. Chen, H.; Yu, P.; Zhang, Z.; Teng, F.; Zheng, L.; Hu, K.; Fang, X. Ultrasensitive self-powered solar-blind deep-ultraviolet photodetector based on all-solid-state polyaniline/MgZnO bilayer. *Small* **2016**, *12*, 5809–5816. [CrossRef]

34. Sun, Z.; Chang, H. Graphene and graphene-like two-dimensional materials in photodetection: Mechanisms and methodology. *ACS Nano* **2014**, *8*, 4133–4156.

35. Mukhokosi, E.P.; Manohar, G.V.; Nagao, T.; Krupanidhi, S.B.; Nanda, K.K. Device architecture for visible and near-infrared photodetectors based on two-dimensional $SnSe_2$ and $MoS_2$: A review. *Micromachines* **2020**, *11*, 750. [CrossRef] [PubMed]

36. Zhang, Y.; Zhao, X.; Chen, J.; Li, S.; Yang, W.; Fang, X. Self-polarized $BaTiO_3$ for greatly enhanced performance of ZnO UV photodetector by regulating the distribution of electron concentration. *Adv. Funct. Mater.* **2020**, *30*, 1907650. [CrossRef]

37. Zhang, L.; Wan, P.; Xu, T.; Kan, C.; Jiang, M. Flexible ultraviolet photodetector based on single ZnO microwire/polyaniline heterojunctions. *Opt. Express* **2021**, *29*, 19202–19213. [CrossRef] [PubMed]

38. Veerla, R.S.; Sahatiya, P.; Badhulika, S. Fabrication of a flexible UV photodetector and disposable photoresponsive uric acid sensor by direct writing of ZnO pencil on paper. *J. Mater. Chem. C* **2017**, *5*, 10231–10240. [CrossRef]

39. Rasool, A.; Kumar, S.; Mamat, M.; Gopalakrishnan, C.; Amiruddin, R. Analysis on different detection mechanisms involved in ZnO-based photodetector and photodiodes. *J. Mater. Sci. Mater. Electron.* **2020**, *31*, 7100–7113. [CrossRef]

40. Hanna, B.; Pillai, L.R.; Rajeev, K.; Surendran, K.; Unni, K. Visible-blind UV photodetectors using a polymer/ZnO nanocomposite thin film. *Sens. Actuator A Phys.* **2022**, *338*, 113495. [CrossRef]

41. Lee, D.J.; Ryu, S.R.; Kumar, G.M.; Cho, H.D.; Kim, D.Y.; Ilanchezhiyan, P. Piezo-phototronic effect triggered flexible UV photodetectors based on ZnO nanosheets/GaN nanorods arrays. *Appl. Surf. Sci.* **2021**, *558*, 149896. [CrossRef]

42. Veeralingam, S.; Yadav, P.; Badhulika, S. An Fe-doped ZnO/BiVO$_4$ heterostructure-based large area, flexible, high-performance broadband photodetector with an ultrahigh quantum yield. *Nanoscale* **2020**, *12*, 9152–9161. [CrossRef] [PubMed]

43. Cao, F.; Jin, L.; Wu, Y.; Ji, X. High-performance, self-powered UV photodetector based on Au nanoparticles decorated ZnO/CuI heterostructure. *J. Alloys Compd.* **2021**, *859*, 158383. [CrossRef]